MAPK scaffolding by BIT1 in the Golgi complex modulates stress resistance

Ping Yi[1,2,3,*], Duc Thang Nguyên[4,*], Arisa Higa-Nishiyama[1,2], Patrick Auguste[2,4], Marion Bouchecareilh[1], Michel Dominguez[5], Regula Bielmann[4], Sandrine Palcy[2], Jian Feng Liu[3] and Eric Chevet[1,2,3,‡]

[1]Avenir, INSERM U889, Bordeaux, France
[2]Université Victor Segalen Bordeaux 2, IFR 66, F-33076, Bordeaux, France
[3]Key Laboratory of Molecular Biophysics of Ministry of Education, School of Life Science and Technology, Huazhong University of Science and Technology, Wuhan, Hubei, China
[4]Department of Surgery, McGill University, Montreal, QC, Canada
[5]HyperOmics Farma, Montreal, QC, Canada

*These authors contributed equally to this work
‡Author for correspondence (eric.chevet@u-bordeaux2.fr)

Accepted 4 January 2010
Journal of Cell Science 123, 1060-1072
© 2010. Published by The Company of Biologists Ltd
doi:10.1242/jcs.059717

Summary

The endoplasmic reticulum (ER) is an essential organelle whose major functions are to ensure proper secretory protein folding and trafficking. These mechanisms involve the activation of specific ER-resident molecular machines, which might be regulated by their membranous environments. Based on this observation, we aimed to characterize the proteome of ER-membrane microdomains to identify new components of the ER that have a role in secretory pathway-associated functions. Using this approach with dog pancreatic rough microsomes, we found that mitochondrial Bcl-2 inhibitor of transcription (BIT1) localized in the early secretory pathway and accumulated in the Golgi complex. Using both a chimeric protein of the luminal and transmembrane domains of ER-resident TRAPα and the cytosolic domain of BIT1, and silencing of BIT1 expression, we perturbed endogenous BIT1 oligomerization and localization to the Golgi. This led to enhanced ERK signaling from the Golgi complex, which resulted in improved stress resistance. This work provides the first evidence for the existence of ER microdomains that are involved in the regulation of BIT1 structure and trafficking, and identifies BIT1 as a negative regulator of the ERK-MAPK signaling pathway in the Golgi.

Key words: BIT1, MAPK, Secretory pathway, Stress

Introduction

The organization of biological membranes into microdomains is now believed to have a key role in cellular processes such as protein targeting and trafficking, and cell signaling (Brown and London, 1998; Ikonen and Simons, 1998). Microdomains from the plasma membrane (PM), which are isolated based on resistance to detergent solubilization, have been identified in almost all mammalian cell types, although they have not been well characterized in other eukaryotes, with the exception of *Saccharomyces cerevisiae* (Kubler et al., 1996) and *Tetrahymena* (Zhang and Thompson, 1997). In the baker's yeast, membrane microdomains detected in the endoplasmic reticulum (ER) were shown to be crucial for the trafficking of several specific proteins such as Gas1p or Pma1p (Bagnat et al., 2000). In addition, in mammalian cells, specific membrane microdomains are essential for retrograde trafficking of Shiga-like toxin from the PM to the ER and cytosol (Smith et al., 2006). Together, these data indicate that the existence of membrane microdomains in the ER might be significantly relevant, at least to membrane and/or protein trafficking. At the PM, the existence of microdomains has been linked to numerous transmembrane receptors signaling and trafficking [e.g. insulin receptor or tumor necrosis factor receptors (TNFRs)] (Bickel, 2002; Doan et al., 2004; Harder, 2004; Legler et al., 2003; Miljan and Bremer, 2002). With regards to the presence of similar structures in the ER, it is of particular interest to underline that TNFR signaling displays some similarities with an ER stress-specific signaling pathway mediated by inositol requiring enzyme 1 (IRE1), because both proteins recruit TNFR-associated factor 2 (TRAF2) upon activation (Schneider-Brachert et al., 2004; Schroder and Kaufman, 2005). Since TNFR signaling and trafficking are regulated by the presence of lipid microdomains (Legler et al., 2003), we postulated that the existence of similar structures in the ER might also have a role in connecting trafficking and signaling in the early secretory pathway.

In the present study, we aimed to identify new components of ER microdomains and characterize their biological function, as well as their potential role in such membranous structures. To this end, we purified ER microdomains, which were then subsequently analysed using proteomics. This led us to demonstrate the presence of the Bcl-2 inhibitor of transcription (BIT1) in ER microdomains. Although this protein was previously reported to localize to mitochondria (Jan et al., 2004), our localization studies revealed the presence of BIT1 in the secretory pathway, and especially its accumulation in the Golgi complex. Interestingly, forced localization of BIT1 in the ER led to the constitutive activation of the ERK-MAPK pathway and subsequent alterations of cell phenotypes.

Our results suggest a role for BIT1 in the early secretory pathway as a key regulator of the ERK-MAPK pathway, which impacts cell adaptation to stress and resistance to death. In addition, these observations highlight the potential role of the Golgi complex as a signaling platform that regulates the life and death decisions of a cell.

Journal of Cell Science

Results

Purification and proteomics analysis of ER microdomains

Previous reports demonstrate that highly specialized microdomain structures are partitioned in the ER membrane similarly to those observed at the plasma membrane. We therefore attempted to enrich ER microdomains from dog pancreatic rough microsomes that were resistant to solubilization by detergents. Dog pancreatic rough ER microsomes were solubilized using either Tween20 (TW) or Triton X-100 (TX) at 4°C. ER microdomains were then isolated by flotation on two successive discontinuous sucrose gradients (Fig. 1A), as reported previously (Bagnat et al., 2000). The resulting fractions were resolved by SDS-PAGE and stained with Coomassie blue R-250. Treatment of ER microsomes with TX led to the almost complete solubilization of the membrane fraction, because no specific protein pattern was observed following Coomassie blue staining of the gel (Fig. 1B). By contrast, solubilization with TW resulted in a specific protein-distribution pattern, suggesting the existence of TW-resistant ER microdomains. Each individual stained band obtained from the TW solubilization was then excised from the gel, reduced, alkylated and trypsin digested before mass spectrometry sequencing (Bell et al., 2001). Among the 103 proteins identified in the ER structures that were resistant to solubilization by TW, nine functional groups were generated (Fig. 1B and supplementary material Table S1) and were represented as follows: (1) translocation (13.7%); (2) protein folding and early post-translational modifications (8.8%); (3) trafficking (7.8%); (4) cytoskeleton organization (5.9%); (5) metabolism (9.8%); (6) signaling (12.7%); (7) cargo proteins (3.9%); (8) translation (4.9%); (9) ribosomal proteins (33.3%). The final group was interesting because membrane microdomains purified by floating were associated with heavy ribosomal moieties (probably the 80S fraction). Out of these 103 proteins, 41.2% were identified as resident in the ER or the ER-Golgi intermediate compartment (ERGIC), whereas 49% were cytosolic (but membrane associated), and 2.5% were proteins from the late secretory pathway. Finally, nine novel proteins or proteins of unknown function were identified, eight of which were predicted to localize in the ER by computational analysis.

Validation of the proteomics analysis and identification of BIT1

As a small number of potential mitochondrial proteins were identified in our proteomics screen, we first monitored the quality of dog pancreatic rough microsomes used in this study. Mitochondrial contamination was ruled out in the present study because rough ER microsomes used for purification of membrane

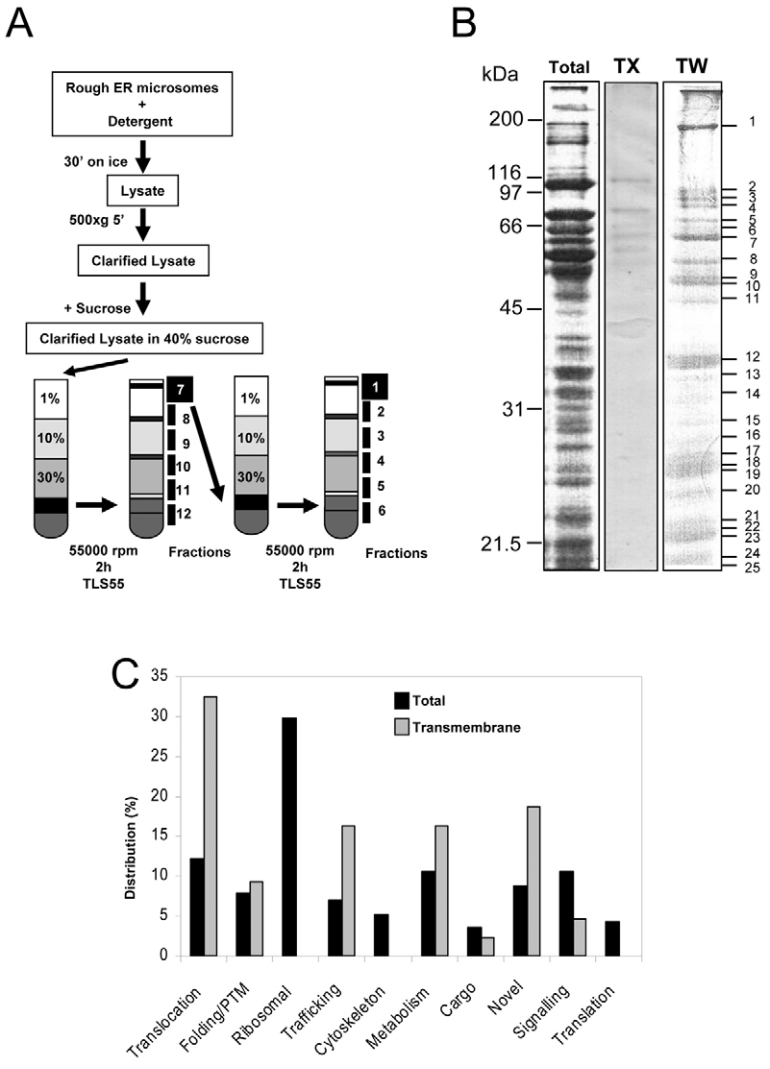

Fig. 1. Purification and proteomics characterization of ER DRMs. (**A**) Schematic representation of DRM isolation. Dog pancreatic rough endoplasmic reticulum microsomes were isolated and solubilized with either Tween 20 (TW) or Triton X-100 (TX). ER microdomains were then isolated by flotation on two successive discontinuous sucrose gradients. (**B**) The resulting fractions were resolved by SDS-PAGE and stained with Coomassie blue R-250. (**C**) Protein composition of Tween 20 DRMs in the ER. Each individual stained band obtained from the Tween 20 solubilization was excised and trypsin digested before mass spectrometry sequencing. Proteins identified (supplementary material Table S1) were categorized into nine functional groups (black bars). Proteins predicted to contain a transmembrane domain were also represented (grey bars).

microdomains showed negligible contamination (<3%) by smooth vesicles (devoid of ribosomes), as demonstrated by a morphological analysis (Fig. 2A). Results obtained through the proteomics analysis were then further validated using an immunoblotting approach. Indeed the presence of four ER-resident or ER-associated proteins (PTP-1B, calnexin, PDI and ORP150) and one ribosomal protein (L4) was monitored in rough ER microsomes and TX- or TW-resistant microdomains. Although in all cases the proteins tested were not or were barely detectable in TX-resistant fractions (Fig. 2B), calnexin and PTP1B were enriched in TW-resistant fractions, whereas no specific enrichment for PDI or L4 and exclusion of ORP150 were observed in those fractions (Fig. 2B). In addition, when the fractions were probed using anti-Tom20 antibodies, no signal was detected in ER (total) microsomes or in detergent-extracted fractions compared with the total particulate (TP) sample (Fig. 2B). Tom-20 was undetectable in our ER microsome preparation, thus reinforcing the above reported EM analysis. Recently, an extensive proteomic analysis of the rat liver secretory pathway has been reported (Gilchrist et al., 2006). Interestingly, we found that more than 55% of the proteins identified (57/103) in our study were also described by these authors (Gilchrist et al., 2006). Moreover, 73% of the remaining proteins identified (n=46) were clearly reported to localize to the ER or ERGIC. Finally, the remaining 17% mostly accounted for pancreas-specific cargo proteins. In an attempt to further evaluate the biological relevance of the protein list identified in the TW-resistant fraction, we reconstituted a functional network using the STRING program suite as described in the Materials and Methods. This led to the construction of a highly connected network (74 nodes and 1483 edges) including 72% of the proteins identified through the proteomics screen (Fig. 2C). This indicates that enrichment of specific proteins in TW-resistant microdomains might be relevant for their functional activity in the ER.

Among the unexpected proteins found in the ER microdomains, we identified BIT1 (PTHR2) (Fig. 2C), a protein that was previously reported to localize in the mitochondria and functions as an apoptosis regulator inhibiting the transcription of Bcl-2 (Jan et al., 2004). Since numerous apoptosis regulators are known to shuttle between the ER and mitochondria (Berridge, 2002; Germain and Shore, 2003; Rudner et al., 2002), the presence of BIT1 in the ER detergent-resistant membranes (DRMs) might be predictive of a trafficking specificity of this protein, as previously demonstrated in *S. cerevisiae* for the role of ER DRMs (Bagnat et al., 2000).

Identification and characterization of BIT1 in the early secretory pathway

BIT1 mRNA derives from a single-exon gene and encodes a protein of 179 residues with a predicted transmembrane domain (residues 15-40) and a predicted cytosolic domain (residues 41-179). Alignment of BIT1 sequences from several organisms showed that this protein is well conserved and displays a particularly conserved region homologous to the peptidyl-tRNA hydrolase PTH2 from *S. cerevisiae* (supplementary material Fig. S1A,B). Although Jan and co-workers (Jan et al., 2004) reported a mitochondrial localization for BIT1, mitochondrial contamination was ruled out in the present

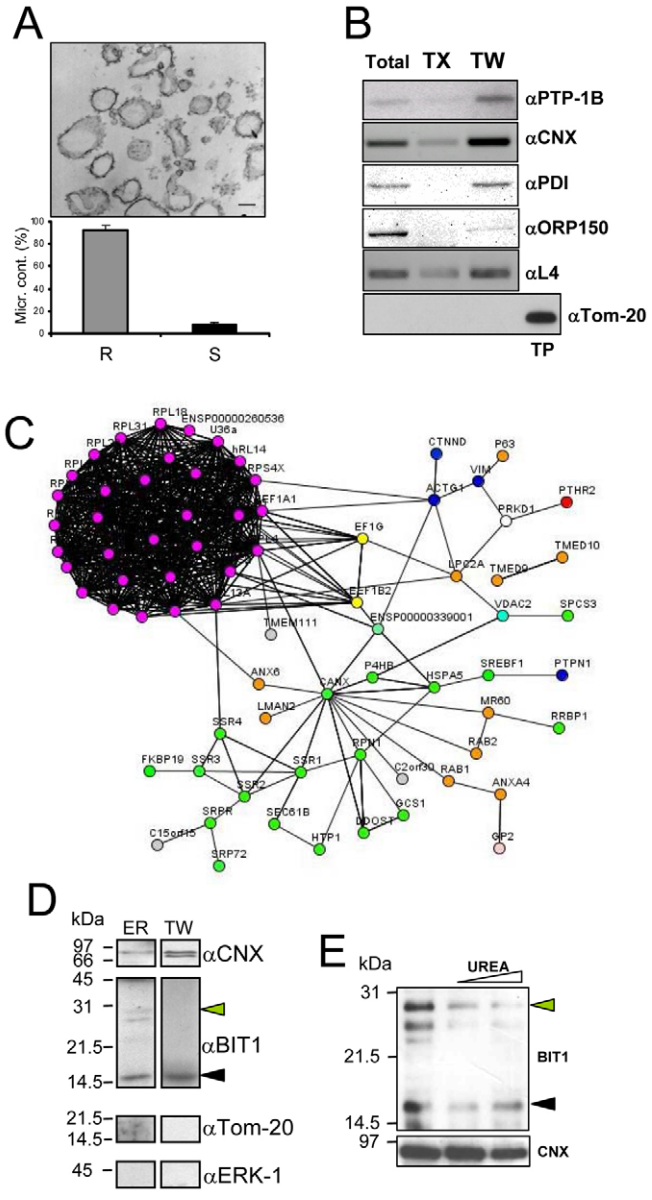

Fig. 2. Quality control of the ER microsomes used for the proteomics analysis and proteomics results. (**A**) Electron micrograph of purified ER microsomes. A representative image is shown (top). Scale bar: 300 nm. The microsome content from ER- and mitochondrial-derived structures was quantified in 20 different images (bottom) corresponding to a total of 1435 microsomes counted. R, endoplasmic reticulum-derived microsomes, S, mitochondria-derived microsomes. (**B**) Immunoblot analysis of sub-ER fractions resistant to TX or TW solubilization. The enrichment of proteins found or not in the proteomic analysis (the protein tyrosine phosphatase 1B, calnexin, protein disulfide isomerase, oxygen regulated protein 150 or ribosomal protein L4) in these fractions. Similarly, the fractions were immunoblotted using anti-Tom20 antibodies; dog pancreas total particulate (TP) was used as positive control. (**C**) Network representation of the proteins identified in our proteomics analysis. This functional network was built using the String program suite (www.string.embl.de) and contains 74 nodes and 1483 edges. Pink, ribosomal proteins; green, ER translocation and folding; blue and brown, signaling and trafficking. (**D**) Purified ER and fractions resistant to TW solubilization were resolved by SDS-PAGE and immunoblotted using the indicated antibodies (Calnexin, BIT1, Tom-20 or ERK-1). The grey and black arrows indicate the position of the 28 kDa and 16 kDa forms of BIT1, respectively. (**E**) Immunoblot analysis of rat liver microsomes treated or not with 4 M and 8 M urea and heated at 60°C for 15 minutes using either anti-BIT1 antibodies (top panel) or anti-calnexin antibodies (bottom panel). The grey and black arrows indicate the position of the 28 kDa and 16 kDa forms of BIT1, respectively.

study (Fig. 2A). To further characterize the distribution of BIT1 in our samples, dog pancreatic ER microsomes and the ER microdomains isolated as in Fig. 1 were immunoblotted using chicken anti-BIT1 antibodies. Two immunoreactive species of ~28 kDa and ~16 kDa were detected (Fig. 2D). The 16 kDa entity was enriched in the sub-ER fractions resistant to TW solubilization and was consistent with the molecular mass of the band in which we initially identified BIT1 (supplementary material Table S1; DPT24). This observation is also consistent with the molecular mass of BIT1 reported by Jan and colleagues (Jan et al., 2004). Both the 28 kDa and 16 kDa forms were confirmed to be BIT1 by mass spectrometry following immunoprecipitation using BIT1 antibodies; the 28 kDa entity was further identified as a potential SDS-resistant dimer of BIT1 because it disappeared upon treatment with 6 M and 8 M urea and heating at 60°C before resolution by SDS-PAGE (Fig. 2E). These data indicated that BIT1 might also localize in the early secretory pathway. This was also reinforced by the enrichment of *BIT1* mRNA in the membrane fractions using a transcriptomic approach (Stitziel et al., 2004). Indeed mRNAs encoding ER-resident and secretory proteins were found to accumulate at their site of translation, most likely by binding ER-bound polysomes.

To evaluate the significance of BIT1 localization to the ER, subcellular localization studies were carried out in cultured cells. First, Fisher Rat 3T3 fibroblasts (FR3T3) were homogenized as described in the Materials and Methods and the post-nuclear supernatant was fractionated into P10 and S10 (pellet and supernatant collected after centrifugation at 10,000 ***g*** for 30 minutes). The latter was further fractionated into P100 and S100 (pellet and supernatant collected after centrifugation at 100,000 ***g*** for 30 minutes). The presence of BIT1 in these fractions was evaluated by immunoblotting. The 28 kDa entity distributed predominantly in the P100, whereas the 16 kDa entity localized exclusively in the P10 fraction (Fig. 3A). As shown by the distribution of the mitochondrial marker Tom20, the Golgi marker MG-160 and the ER marker calnexin, P100 mainly contained ER and some Golgi, whereas P10 contained ER, Golgi and mitochondria (Fig. 3A). BIT1 was never detected in the cytosolic fraction (S100), thus indicating that BIT1 is always membrane associated. Second, an immunocytochemistry analysis was carried out in the human liver cancer cell line HuH7 using anti-BIT1 antibodies (Fig. 3B). This analysis unexpectedly revealed that in whole cells, BIT1 did not localize to the mitochondria (using Mitotracker as a mitochondrial marker) (Fig. 3B, top panels). Moreover, BIT1 localization to the ER was not detectable using this approach with calnexin as an ER marker (Fig. 3B, middle panels). Finally, except for an intense nuclear staining, which was nonspecific (as shown in supplementary material Fig. S2), BIT1 did not localize in the cytoplasm, but was enriched in the Golgi complex, as indicated by the overlapping staining observed with the Golgi marker giantin (Fig. 3B, bottom panels). To further evaluate the localization of BIT1 in the secretory pathway, we purified ER and Golgi fractions from rat liver, as previously described (Bell et al., 2001; Gilchrist et al., 2006). These fractions were either directly resolved by SDS-PAGE or membrane microdomains were extracted using Tween solubilization before SDS-PAGE and immunoblotting with anti-BIT1, anti-MG160 and anti-CNX antibodies. This revealed that BIT1 was present in membrane microdomains in the Golgi complex and that most BIT1 was in monomeric conformation (Fig. 3C).

Constitutive expression of BIT1 in the ER alters endogenous BIT1 trafficking to the Golgi

To further study the role of BIT1 and investigate its previously described pro-apoptotic functions (Jan et al., 2004) in the secretory pathway, we generated a fusion protein in which the BIT1 cytosolic

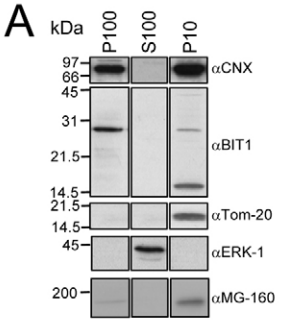

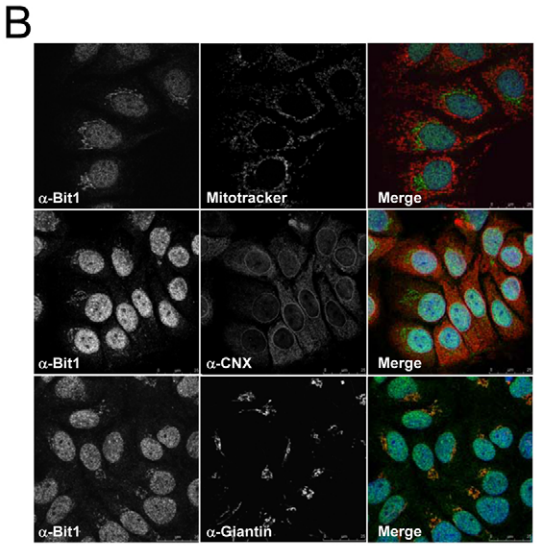

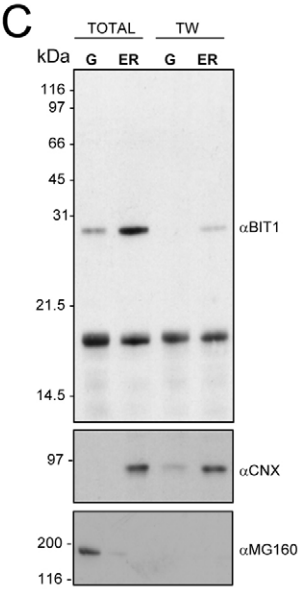

Fig. 3. Localization of BIT1 in the secretory pathway. (**A**) FR3T3 cells homogenized and separated into P10, P100 and S100 fractions. Equal amounts of each fraction were separated on SDS-PAGE and immunoblotted with the indicated antibodies. (**B**) Confocal microscopy analysis of BIT1 localization in HuH7 cells using anti-BIT1, anti-calnexin (CNX), anti-giantin antibodies and Mitotracker. (**C**) Immunoblot analysis of rat liver Golgi and ER fractions either total or TW extracted using anti-BIT1 antibodies, anti-CNX antibodies and anti-MG160 antibodies.

Journal of Cell Science

domain replaced the cytosolic domain of the ER-resident transmembrane protein Trapα (which was also found in the DRM fraction in this proteomics approach, supplementary material Table S1). The resulting fusion protein, C-terminally Myc-tagged Trap.BIT1, consisted of the putative BIT1 cytosolic domain fused downstream to the luminal and transmembrane domains of Trapα and was expressed from pcDNA3.myc with a predicted molecular weight of 43 kDa (supplementary material Fig. S3). Trapα luminal and transmembrane domains (TrapLT, without the cytosolic domain) cloned in pcDNA3.myc and full-length pcDNA3.BIT1 were used as controls. The expression of the Trap.BIT1 transgene was first assessed in COS7 cells transiently transfected with pcDNA3.Trap.BIT1 for 24 hours and 48 hours, followed by immunoprecipitation from the precleared lysates using anti-myc antibodies. Immunoblotting with the anti-BIT1 antibodies revealed the presence of a protein at the predicted molecular weight (~43 kDa), which increased over time and which was absent in the mock-transfected cells (supplementary material Fig. S3), thus confirming that the anti-BIT1 antibodies are specific to BIT1.

Trap.BIT1 proteins stably expressed in FR3T3 cells were separated in P10, P100 and S100 fractions after homogenization of individual clones of each construct, followed by immunoblotting with anti-BIT1 antibodies. The distribution of BIT1 in FR3T3 cells expressing stably BIT1 (Fig. 4A,B) was similar to that of non-transfected cells with a predominant localization of the 28 kDa entity in the P100 and an exclusive localization of the 16 kDa form in the P10 fraction. Unexpectedly, when FR3T3 cells were stably transfected with Trap.BIT1, Trap.BIT1 was found exclusively in the P10 fraction (Fig. 4A,B). In both cell types, Trapα and calnexin were found to distribute in both P100 and P10 fractions, whereas the Golgi marker MG160 mostly distributed in the P10 fraction, with some remnants in the P100 fraction (Fig. 4A,B). Most interestingly, upon stable expression of Trap.BIT1 in these cells, even at levels lower than that of endogenous BIT1, the 16 kDa form of endogenous BIT1 was barely detectable in the P10 fraction (Fig. 4B). This result suggests that Trap.BIT1 prevents BIT1 from exiting the ER under monomeric configuration.

To investigate whether Trap.BIT1 prevents the exit of endogenous BIT1 from the ER and consequently block its functions in the Golgi, we first tested whether expression of Trap.BIT1 led to the expected phenotypes observed in *BIT1*-silenced cells (Jan et al., 2004). Cells expressing stably the different transgenes were grown in suspension for 24-96 hours and apoptosis was measured. FR3T3 cells stably transfected with pcDNA3 alone or pcDNA3.TrapLT showed a moderate increase in apoptotic cells (20% and 13%, respectively, after 48 hours). By contrast, detachment induced a higher level of apoptosis in BIT1 expressing cells (45%, after 48 hours). Notably, the expression of Trap.BIT1 led to a significantly lower level of apoptosis than in cells expressing BIT1 (6% vs 45%, respectively, after 48 hours) (Fig. 4C). These results confirmed that overexpression of wild-type BIT1 has a proapoptotic potential, as previously shown (Jan et al., 2004), whereas Trap.BIT1 expression might lead to a reduced sensitivity towards anoikis (Fig. 4C). This

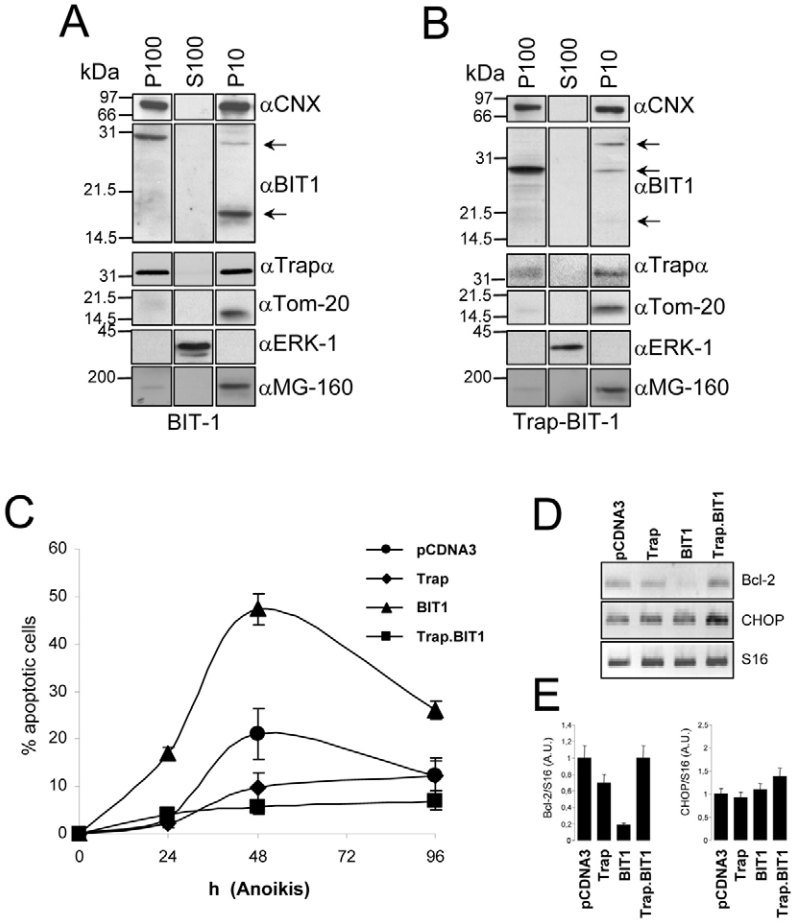

Fig. 4. Modulation of endogenous BIT1 activity. Individual clones of FR3T3 cells stably expressing full-length BIT1 (**A**) or Trap.BIT1 (**B**) from pcDNA3 were homogenized and post-nuclear supernatants were separated into P10 and P100 fractions. These were then resolved by SDS-PAGE and immunoblotted using the indicated antibodies. The experiment was repeated at least three times on two independent clones. A representative immunoblot is shown. Arrows indicate the position of the 28 kDa and 16 kDa forms of BIT1 as well as the trap.BIT1 protein (top arrow right panel). (**C**) Individual clones of FR3T3 cells stably transfected with pcDNA3 (Ctrl), pcDNA3.Trap, BIT1 or Trap.BIT1 were grown in suspension for 24, 48 and 96 hours. At each time point, the percentage of apoptosis was measured (n=2, value ± 0.5 variation). (**D**) RT-PCR analysis of expression of mRNA encoding Bcl-2, CHOP and S16 in FR3T3 cells stably transfected with the indicated constructs under basal conditions. A representative agarose gel of the RT-PCR assay is shown (n=3). (**E**) Quantification of the RT-PCR experiments obtained in D.

observation was further validated when the expression of *BCL2* mRNA was evaluated. In cells overexpressing wild-type BIT1, the expression of *BCL2* mRNA was dramatically reduced under basal conditions, confirming the results previously reported (Jan et al., 2004); however, such a reduction was not observed in cells expressing Trap.BIT1 (Fig. 4D and quantification in Fig. 4E). These results suggest that Trap.BIT1 prevents BIT1 function, most likely by affecting its exit from the ER under monomeric conformation.

Trap.BIT1-mediated cellular phenotypes

Cells expressing BIT1 and Trap.BIT1 exhibited a significantly slower growth rate than the other cell types tested (Fig. 5A). Because the observed impact on anoikis might correlate with the initial findings that apoptosis mediated by a loss of cell attachment to the extracellular matrix involves BIT1 (Jan et al., 2004), we investigated the consequences of absence of substrate on these four cell types (Fig. 5B; supplementary material Fig. S4). Cells expressing TrapLT or full-length BIT1 were similarly unable to grow on soft agar, similarly to cells transfected with the empty vector. In stark contrast, Trap.BIT1-expressing cells were able to grow in an anchorage-independent manner (Fig. 5B). To elucidate the potential consequences of constitutive expression of BIT1 in the ER, pCDNA3 TrapLT, BIT1 and Trap.BIT1 cell lysates were immunoblotted using antibodies raised against various proteins involved in major survival and death signaling cascades (see Materials and Methods). Interestingly, the constitutive activation of MEK-1 and ERK1/2 was observed in Trap.BIT1 cells (Fig. 5C). This result correlates nicely with the previously reported observation that BIT1-knockout mice display high levels of ERK1 phosphorylation (Kairouz-Wahbe et al., 2008). Interestingly, when the phosphorylation of RAF1 and B-RAF was monitored in these cells, a weak phosphorylation of B-RAF was detected only in Trap.BIT1 cells (Fig. 5D). The expression and phosphorylation levels of other signaling intermediates (MKK7, JNK, SMAD2, AKT) were also tested in the four cell types under basal conditions

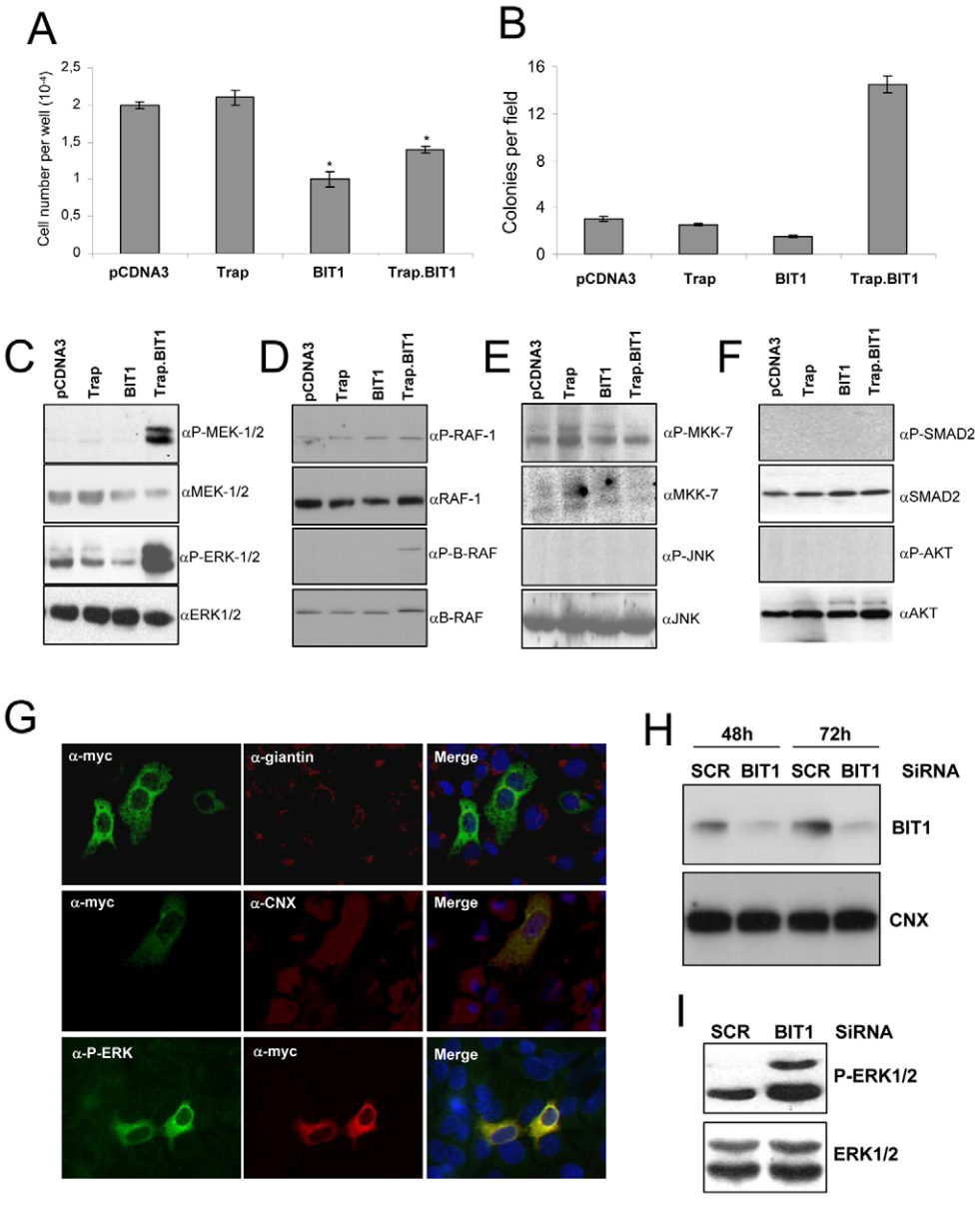

Fig. 5. FR3T3 phenotype modulation upon BIT1 mutant expression. (**A**) FR3T3 cells stably transfected with pcDNA3, pcDNA3.Trap.LT, pcDNA3.BIT1 or Trap.BIT1 were counted after growth for 4 days on regular culture dishes in DMEM with 10% FBS (n=3; mean ± s.d.). (**B**) Cells from A were grown on soft agar for 2-3 weeks. The experiment was done twice on two independent clones. Quantification of the number of colonies from ten different fields obtained from the soft agar assay is reported. (**C**-**F**) Precleared lysates from FR3T3 cells stably transfected with pcDNA3, pcDNA3.Trap.LT, pcDNA3.BIT1 or Trap.BIT1 and grown on regular culture dishes with 10% FBS resolved by SDS-PAGE and immunoblotted with the indicated antibodies (results are representative of three experiments). (**G**) Immunodetection of Trap.BIT1 in HuH7 cells transiently transfected using epifluorescence microscopy. The colocalization study is performed with the ER marker calnexin (CNX), the Golgi marker giantin and anti-phospho-ERK antibodies. (**H**) HuH7 cells transfected with either a scrambled (SCR) siRNA or a siRNA against *BIT1*. Total proteins were then immunoblotted using anti-BIT1 antibodies and anti-CNX antibodies. (**I**) Phosphorylation and expression status of ERK1/2 in immunoblots of control and *BIT1*-knockdown HuH7 cells.

(Fig. 5E,F). No significant change in either phosphorylation or expression was observed. As a consequence, and to test whether ERK activation correlated with the expression of Trap.BIT1, HuH7 cells were transiently transfected with Trap.BIT1 expression vector and the expression and localisation of this protein was evaluated by immunofluorescence using anti-MYC antibodies, anti-CNX (for ER staining) and anti-Giantin (for Golgi staining). Trap.BIT1 localized in the ER as expected (Fig. 5G, top and middle panels). In addition, when we monitored ERK phosphorylation in those cells, we observed that increased phosphorylation of ERK was present exclusively in Trap.BIT1-transfected cells (Fig. 5G, bottom panel). To confirm the hypothesis that the absence of BIT1 could lead to enhanced MAPK activation, a siRNA-based approach was carried out. BIT1 protein expression was reduced to approximately 25-35% of its initial levels using previously described siRNA sequences (Jan et al., 2004) (Fig. 5H) and this led to enhanced phosphorylation and activation of the MAPK pathway (Fig. 5I), thus agreeing with the Trap.BIT1- and BIT1-knockout data (Kairouz-Wahbe et al., 2008). These data demonstrate that the impairment of BIT1 expression or localization leads to the enhancement of MAPK signaling.

The localization of Trap.BIT1 in HuH7 cells was further monitored in stably transfected cells using immunofluorescence and confocal microscopy (Fig. 6). As expected, Myc signals were not detected in mock-transfected cells (Fig. 6A); by contrast, in Trap.BIT1-transfected cells, a strong ER staining was observed with anti-MYC antibodies, which strongly co-localized with the ER marker calnexin (Fig. 6B, middle panel). Interestingly, a weak co-localization of Trab.BIT1 with the Golgi marker giantin was also observed (Fig. 6B, bottom panels) and no colocalization with the mitochondrial marker mitotracker was detected (Fig. 6B, top panel). These results indicate that Trap.BIT1 molecules mostly localize in the ER, which could lead to the subsequent alteration of MAPK signaling.

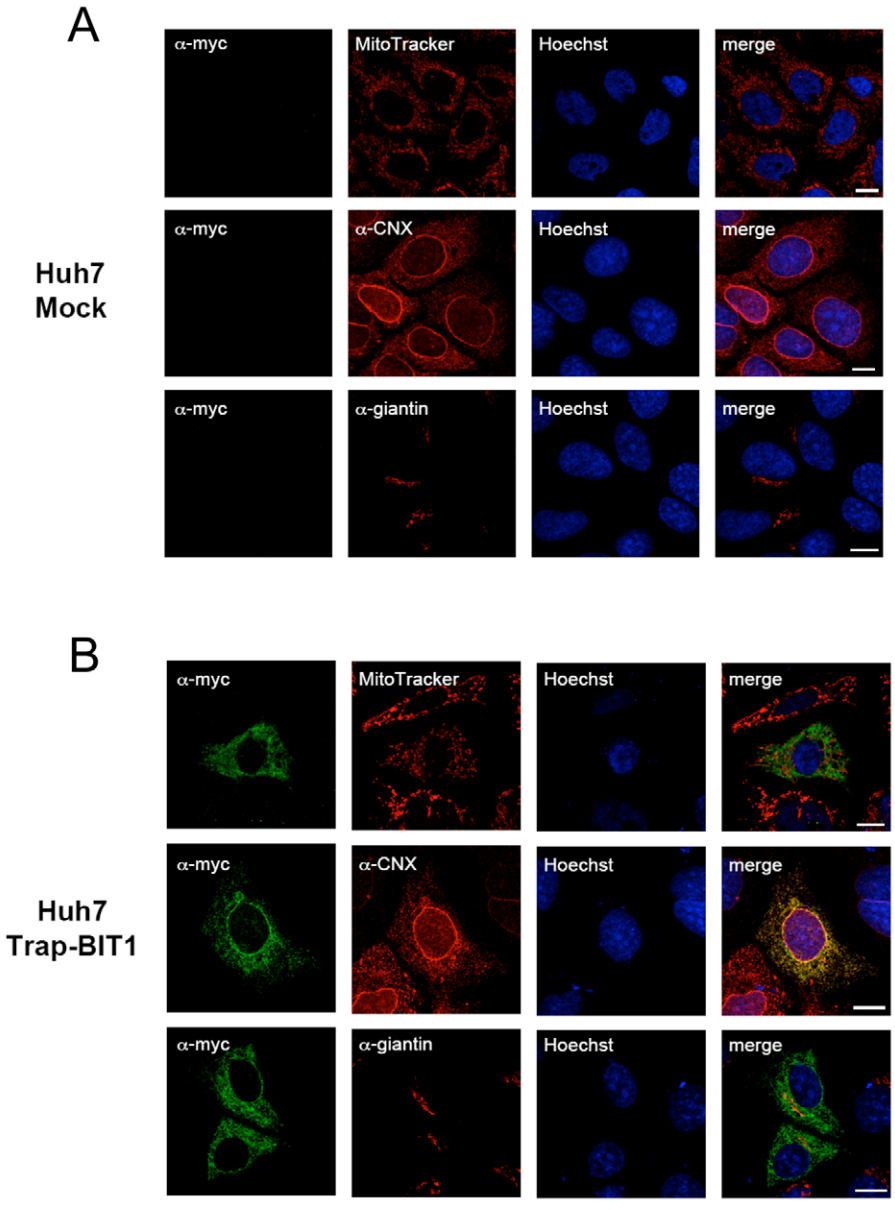

Fig. 6. Trap.BIT1 proteins localize mostly in the ER. (**A**,**B**) Confocal microscopy analysis of HuH7 mock-transfected cells (A) and HuH7 cells stably expressing Trap.BIT1 (B) using anti-MYC, anti-CNX and anti-Giantin antibodies and Mitotracker. Scale bars: 10 μm.

Journal of Cell Science

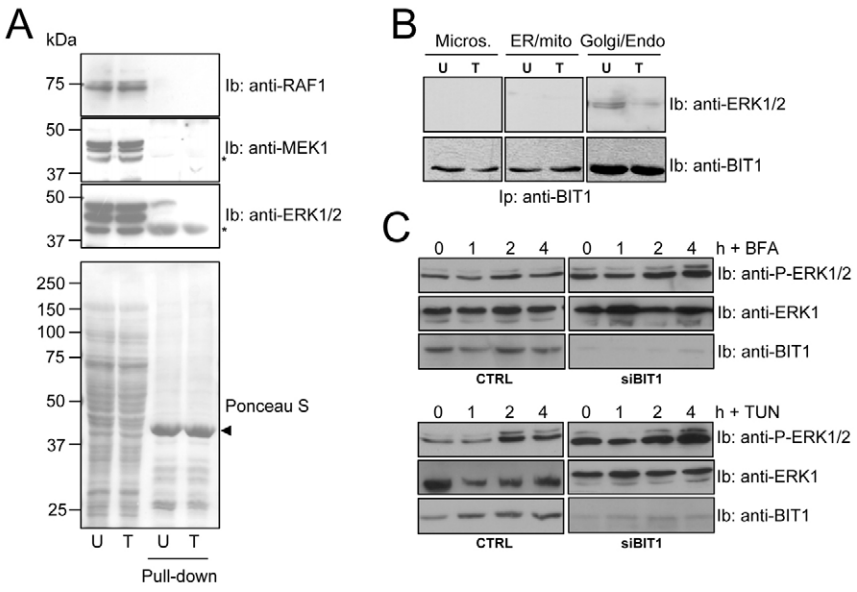

Fig. 7. BIT1 expression regulation and interaction with the MAPK pathway. (**A**) GST-BIT1 pull-down carried out on total liver lysates extracted from mice treated (T) or not (untreated; U) with tunicamycin (0.1 μg/g body weight) for 6 hours. A Ponceau S stain of the nitrocellulose membrane obtained after separation of the pulled down material by SDS-PAGE and transfer is shown (bottom). Membranes were immunoblotted using the indicated antibodies. A representative experiment of three is shown. (**B**) Membrane fractionation of mouse liver collected following tunicamycin treatment. Membrane fractions (total microsomes, ER-mito, Golgi-endosomes; 100 μg) solubilized using 1.5% CHAPS and subjected to immunoprecipitation using anti-BIT1 antibodies. Immunoprecipitates were resolved by SDS-PAGE, transferred to nitrocellulose membranes and immunoblotted using anti-ERK1/2 antibodies. The experiment was carried out in duplicate. (**C**) Time-course analysis of ERK phosphorylation in HuH7 control cells or cells silenced for *BIT1* expression and treated with either brefeldin A (BFA, top panel) or tunicamycin (TUN, bottom panel).

BIT1 expression regulation and interaction with the MAPK module

The above-mentioned results suggested that BIT1 could interfere with MAPK signaling owing to its subcellular localization. We consequently tested the potential interaction of BIT1 with the MAPK module using a GST-BIT1 pull-down approach. This was carried out using liver extracts from mice subjected to ER stress, because this was previously shown to affect both the secretory pathway and MAPK activation (Nguyen et al., 2004). The N-glycosylation inhibitor tunicamycin was selected as a stress inducer and liver extracts were prepared from three mice treated with this antibiotic and three mice treated with DMSO. GST-BIT1 was then carried out, and the association of BIT1 with the ERK-MAPK pathway, namely RAF1, MEK1 and ERK1/2, was evaluated by immunoblot (Fig. 7A). This revealed that BIT1 was able to bind mainly to ERK1, independently of MEK1 and RAF1, only under basal conditions (Fig. 7A). We further investigated the BIT1-ERK1 complex in liver organelles. To this end, subcellular fractionation was carried out on total cell extracts using isopycnic sucrose gradient sedimentation. Fractions corresponding to total microsomes, ER/mitochondria and Golgi or endosomes were solubilized, followed by immunoprecipitation using anti-BIT1 antibodies. Immunoprecipitates were then resolved by SDS-PAGE, transferred to nitrocellulose and immunoblotted using both anti-ERK1/2 and anti-BIT1 antibodies (Fig. 7B, top and bottom panels respectively). These results confirmed that BIT1 formed a complex with ERK1 in the Golgi and that this complex was disrupted upon ER stress. To further evaluate the contribution of BIT1 in the activation of the MAPK pathway, *BIT1* expression was silenced in HuH7 cells, which were then treated either with brefeldin A (BFA) or tunicamycin (Fig. 7C). Our results showed that ERK activation was induced in control and siBIT1 cells upon tunicamycin treatment (Fig. 7C, bottom panel). By contrast, ERK activation upon BFA treatment was observed only in *BIT1*-silenced cells, not in control cells (Fig. 7C, top panel). Our results indicate that BIT1 participates in the regulation of MAPK activity in the Golgi. Our next step was to assess the physiological relevance of BIT1 functionality and MAPK activation.

BIT1 negatively regulates the activation of the MAPK module in the Golgi

As the activation of the MAPK module is triggered from various spatial locations including the Golgi (Inder et al., 2008; Lunin et al., 2004), we postulated that BIT1 localization and/or oligomeric status and/or BIT1 expression represent a regulatory parameter in this activation process. To further test the hypothesis that BIT1 localization regulates the activation of the MAPK module in intracellular organelles, HuH7 mock-transfected and Trap.BIT1-tranfected cells were then analyzed by immunofluorescence microscopy for the localization of phosphorylated ERK. This was found to be localized in the cytoplasm, but was also enriched in the periphery of the nucleus – an area that was co-labelled with anti-giantin antibodies, thus showing a Golgi localization in both cell types (Fig. 8A). When a confocal microscopy analysis of these cells was carried out, we observed that phosphorylated ERK and giantin co-localized in cells stably expressing Trap.BIT1, but not in mock-transfected cells (Fig. 8B, left panels). This colocalization disappeared upon BFA treatment, but ERK phosphorylation remained more intense in Trap.BIT1 cells (Fig. 8B, right panels), thus agreeing with data shown in Fig. 7C.

In an attempt to quantify this observation, the percentage of cells presenting phosphorylated ERK and giantin co-localization was determined. Interestingly, levels of co-localization of these proteins in Trap.BIT1 cells were 2- to 3-fold greater than levels observed in control cells (Fig. 8C, left panel). This suggested that the normal localization of BIT1 in the Golgi prevents the activation of the ERK-MAPK module from this compartment. In addition, we noticed that in Trap.BIT1 cells, the Golgi was approximately half the size of that in control cells (Fig. 8C, right panel). Similar data were also observed upon silencing of *BIT1* expression (Fig. 8D, right and left panels respectively). These data demonstrate that BIT1 negatively regulates activation of MAPK when present in the Golgi.

BIT1 regulates MAPK-mediated stress resistance

We first investigated the ability of Trap.BIT1-expressing cells to survive upon tunicamycin-induced ER stress. Indeed, we found that *BIT1* expression was upregulated upon tunicamycin-induced

Journal of Cell Science

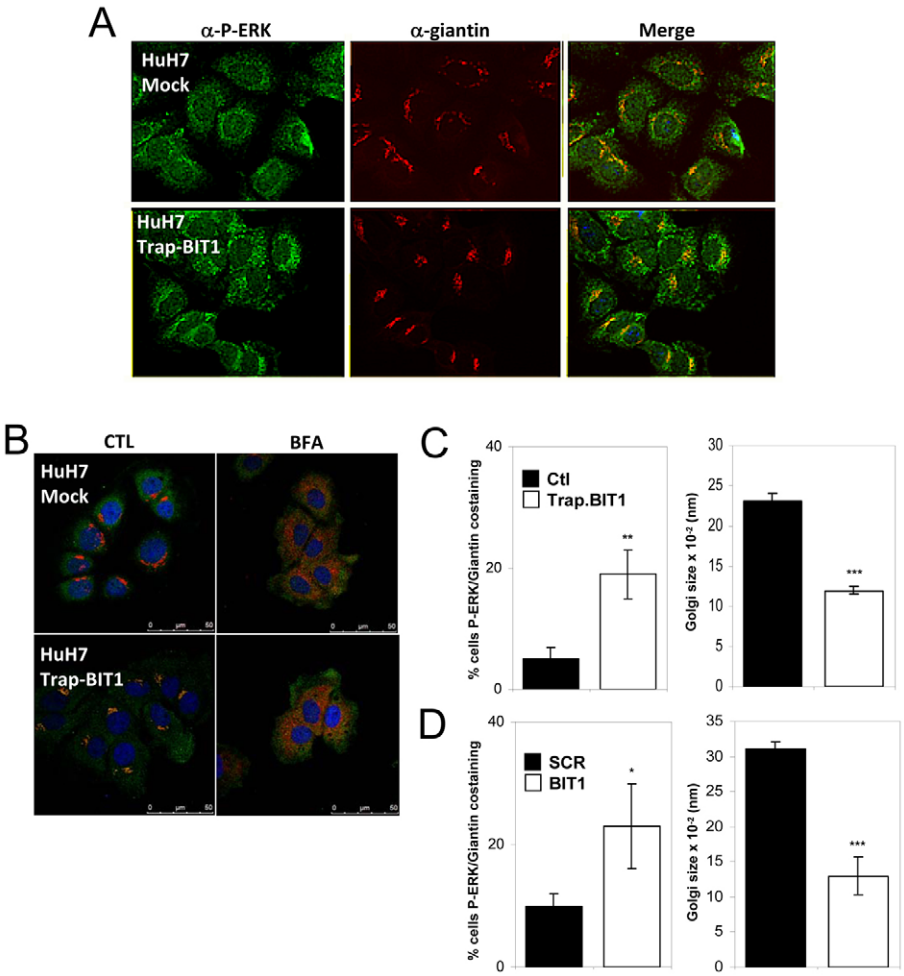

Fig. 8. Constitutive expression of BIT1 in the ER alters cell MAPK signaling. (**A**) Immunofluorescence analysis carried out in mock-transfected HuH7 cells (top panels) or Trap.BIT1 stably transfected cells (bottom panels) using anti-MYC, anti-giantin and anti-CNX antibodies. (**B**) Confocal analysis carried out in mock-transfected HuH7 cells or Trap.BIT1 stably transfected cells treated or not with BFA using anti-phospho-ERK and anti-giantin antibodies. (**C**) Quantification of cells displaying phospho-ERK and giantin co-staining (left) and average size (periphery) of Golgi complex (right) in HuH7 cells transfected with an empty vector or a vector bearing the Trap.BIT1 construct. (**D**) Quantification of cells displaying phospho-ERK and giantin co-staining (left) and average size (periphery) of Golgi complex (right) in HuH7 cells transfected with scrambled siRNA or *BIT1* siRNA. For determination of phosphorylated ERK in the Golgi, at least 300 cells were counted in three independent experiments. The Golgi periphery was determined in 50 cells in three independent experiments. Values represent mean ± s.d. (**P*<0.05, ***P*<0.02, ****P*<0.01; Student's *t*-test).

ER stress and impairment of BIT1 functionality led to enhanced MAPK activation; we thus predicted that BIT1 could be part of a pro-death program that is induced upon ER stress. Consequently, impairment of BIT1 functionality, by either localization or silencing, might lead to enhanced survival. This was indeed the case, because Trap.BIT1-expressing FR3T3 cells were more resistant to tunicamycin treatment than any of the control cells (transfected with mock vector, Trap or BIT1) (Fig. 9A). Similar results were obtained in HuH7 cells using both the Trap.BIT1 stable cell line and cells transfected with *BIT1* siRNA (Fig. 9B), thus validating our initial hypothesis. To further test whether this phenomenon was related to the high MAPK activation level observed under impairment of BIT1 functionality, similar experiments were carried out in the presence of the MEK1 inhibitor PD98059. Interestingly, although PD98059 did not have a major effect on the survival of either control or *BIT1*-transfected cells, this chemical completely abrogated the resistance of *BIT1*-silenced cells to tunicamycin-induced death (Fig. 9C). This suggested that BIT1-mediated regulation of the MAPK pathway upon ER stress could significantly contribute to cell death and provides a new role for BIT1 as a pro-apoptotic agent.

Discussion

In this study, we have used a sub-organellar proteomics approach to enrich new components of this organelle. Our efforts focused on purifying membrane microdomains from the ER. This led us to identify BIT1, a protein previously reported to localize to mitochondria (Jan et al., 2004), which we found to be enriched in ER membrane microdomains, most likely en route to its final destination in the Golgi. This led us to the discovery of a new mechanism for BIT1 in the Golgi, where it negatively regulates MAPK activation, prevents adaptation and promotes cell death upon stress. We discuss below the functional implications of this discovery.

BIT1 localization in the secretory pathway

Enrichment of TW-resistant ER microdomains is thought to be similar to what happens at the PM, where signaling or trafficking initiators can be conditioned by the existence of specific membrane microdomains. As a consequence, we searched for proteins in TW-resistant ER microdomains that might function as signaling intermediates. The nature of membrane microdomains in the ER would be expected to significantly differ from those found at the PM, because cholesterol is enriched at the PM and present at very low levels in the ER. We anticipated that ER microdomains would contain less cholesterol that those purified from PM, so we used Tween20 to extract ER microdomains rather that Triton X-100, which is commonly used for PM extractions. Interestingly, besides the tyrosine phosphatase PTP-1B, which was previously found to potentiate IRE1 signaling in the ER (Gu et al., 2004), the only

Journal of Cell Science

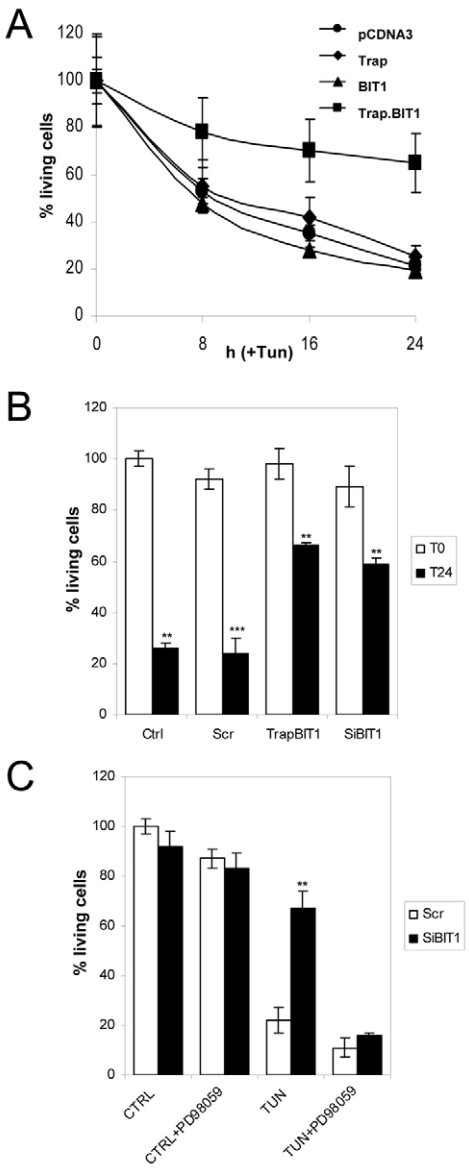

Fig. 9. Functional impact of BIT1-mediated MAPK regulation. (**A**) Individual clones of FR3T3 cells stably transfected with pcDNA3 (Ctrl), pcDNA3.Trapα LT, pcDNA3.Bit-1 or Trap.Bit-1 were grown on regular culture dishes in DMEM and 10% FBS in the presence of 10 µg/ml tunicamycin over a period of 24 hours. At the times indicated, the percentage of living cells was determined. The experiment was repeated three times and data are mean ± s.d. of the three repeats. (**B**) Comparison of the impact of TrapBIT1 expression and *BIT1* silencing on HuH7 resistance to tunicamycin following treatment for 24 hours with 5 µg/ml. The experiment was carried out in triplicate and the mean ± s.d. is shown. (**C**) Impact of BIT1-dependent MAPK activity on HuH7 resistance to tunicamycin treatment. HuH7 cells transfected with scrambled (Scr) siRNA or *BIT1* siRNA were treated with tunicamycin (5 µg/ml) in the absence or presence of 50 µM PD98059. Cell survival was monitored after 24 hours. The experiment was carried out three times and is shown as the mean ± s.d. (**P*<0.05, ***P*<0.02, ****P*<0.01; Student's *t*-test).

identified protein whose function was directly related to signaling events was the Bcl2 inhibitor of transcription 1 (BIT1). This protein had previously been reported to localize to mitochondria (Jan et al., 2004) and is involved in anoikis by preventing the upregulation of *BCL2* transcription. This observation led us to confirm the presence of BIT1 in the ER by assessing the mitochondrial contamination level of our initial dog pancreatic ER preparations. When all the smooth vesicles were counted as contaminants, this amount remained below 3% of total microsomes, thus indicating that our observation was accurate. Moreover, only one mitochondrial protein was identified by mass spectrometry sequencing (supplementary material Table S1). Moreover, other large-scale proteomics analyses of the secretory pathway revealed the presence of BIT1 in the secretory pathway (Gilchrist et al., 2006). Finally, our results were also confirmed by BIT1 localization studies in cultured cells. Indeed, BIT1 was enriched in the Golgi and no co-localization was found when Mitotracker was used as a mitochondrial marker (Fig. 2). This result was in accordance with previously reported observations indicating that lipid microdomains in the ER are important for protein trafficking through the secretory pathway (Bagnat et al., 2000). We were not able to reproduce the observation made by Jan and co-workers (Jan et al., 2004) who showed the almost exclusive localization of BIT1 to mitochondria, even though we analyzed the endogenous BIT1 or a MYC-tagged recombinant protein. This discrepancy is probably due to the biological models used in our study (purified ER and Golgi microsomes, FR3T3 and HuH7 cells) whereas HeLa cells were used by Jan and colleagues.

BIT1-dependent signaling

To measure the functional impact of BIT1 in the secretory pathway, we specifically targeted this molecule to the ER by generating a fusion protein between the luminal and transmembrane domains of Trapα and the cytosolic domain of BIT1. A similar approach had already been successfully used with Bcl-2 to demonstrate its ER-associated functions (Foyouzi-Youssefi et al., 2000). Cells expressing Trap.BIT1 presented an endogenous BIT1 expression pattern that was different to that of control cells (Fig. 4); in addition, we showed that Trap.BIT1 proteins mostly resided in the ER (Fig. 6). Indeed, the 16 kDa entity was not detected in the former, probably because BIT1 was unable to exit SDS-resistant complexes. We consequently postulated that Trap.BIT1 impairs normal localization of endogenous BIT1 function by retaining it in the ER. This hypothesis was in part confirmed by the fact that BIT1 mostly existed as monomeric entities in the Golgi (Fig. 3). Interestingly, Trap-BIT1 cells, although showing minor defects in cell growth, were able to form colonies in soft agar, demonstrating a role for Trap.BIT1 in the activation of pro-survival pathways, either as a consequence of the absence of the 16 kDa form of BIT1 and/or of the presence of the expression of the Trap.BIT1 fusion in the ER.

The molecular consequences of BIT1 retention in the ER, although having specific impact on cell phenotypes, remain unclear. In the hypothesis of a Trap.BIT1-mediated impairment of the role of endogenous BIT1, we tested the impact of Trap.BIT1 expression on the previously reported observation that in BIT1$^{-/-}$ cells, the ERK/MAPK pathway was hyperactivated (Kairouz-Wahbe et al., 2008). As expected, phosphorylation levels of both MEK-1 and ERK1/2 were highly increased in Trap.BIT1 cells compared with the three other cell lines tested. In addition, our data show that BIT1 might act to prevent the activation of the MAPK module from the Golgi (Figs 7-9) because the expression of dominant-negative Trap.BIT1, which correlated with altered expression of the 16 kDa entity (monomeric BIT1), led to enhanced Golgi localization of phosphorylated ERK. Interestingly, it was recently demonstrated

Journal of Cell Science

that the protein kinase PKD1 modulates BIT1 activity (Biliran et al., 2008). As PKD was previously reported to modulate ERK activation (Brandlin et al., 2002; Wong and Jin, 2005), we therefore postulate that PKD1 modulates ERK activation through BIT1. This observation could also fit with a model where this regulatory network, involving ERK, PKD1 and BIT1, controls Golgi structure and size, as previously reported separately for ERK (Inder et al., 2008; Lunin et al., 2004; Mor and Philips, 2006; Morgado-Diaz et al., 2007; Philips, 2004) and PKD (Ghanekar and Lowe, 2005; Hausser et al., 2005; Sanchez-Ruiloba et al., 2006) proteins.

BIT1, stress resistance and cell death

In previous reports, BIT1 was demonstrated to be a crucial apoptosis regulator through its role on the expression of BCL2 expression (Jan et al., 2004), MAPK regulation (Kairouz-Wahbe et al., 2008) or through its role on TAp63γ (Fan et al., 2009). In the present report, we demonstrate that the role of BIT1 on MAPK activation could occur in the secretory pathway and more particularly in the Golgi, as already demonstrated for Sef proteins (Philips, 2004), and thus BIT1 selectively prevents the activation of specific downstream targets. Interestingly, our data suggest that BIT1 could also act through the inhibition of B-Raf (Fig. 5D) and consequently might have a scaffolding role for B-Raf, MEK1 and ERK1/2. Moreover, the role of BIT1 in the Golgi complex could also be further reinforced by the recent observation that PKD1 is a positive regulator of the apoptotic functions of BIT1 (Biliran et al., 2008), because PKD1 has also been shown to have a significant role in Golgi functions.

In this work, we report that the protein BIT1 localizes to the early secretory pathway and is enriched in the Golgi. Constitutive localization of BIT1 in the ER leads, in turn, to the basal activation of ERK signaling and enhanced resistance to anoikis. This observation correlated with enhanced localization of phosphorylated ERK in the Golgi and reduced Golgi size. Our work might therefore reveal a key regulatory mechanism for the balance between pro-survival and pro-apoptotic pathways via BIT1 and its subcellular localization, through the control of MAPK signaling from the Golgi.

Materials and Methods

Antibodies and reagents

Anti-calnexin (CNX) antibodies were a kind gift from John Bergeron (McGill University, Montreal, Canada). Anti-MYC antibodies were purchased from Cell Signaling. HiFi Taq Polymerase and LR recombinase were from Invitrogen. Complete™ Protease inhibitors were purchased from Roche. The predicted cytosolic domain of BIT1 (residues 41-179) was PCR amplified from a human liver cDNA library with HiFi polymerase and the primers 5′-GGG GAC AAG TTT GTA CAA AAA AGC AGG CTT GCC CAA AAG CAA GAC GAG CAA G-3′ and 5′-GGG GAC CAC TTT GTA CAA GAA AGC TGG GTC TAG TAA AGT TTT AGG TGA CCA GTG ACT TTG TC-3′. The amplified fragment was then recombined into pGEX2TK that was previously made GATEWAY® compatible (Invitrogen) to generate pGEX2TK.BIT1 encoding BIT1 (residues 41-179) fused downstream of GST. Expression of GST.BIT1 by exponentially growing DH5α bacteria transformed with pGEX2TK.BIT1 was induced with 1 mM IPTG for 5 hours, GST.BIT1 was purified from the lysate using glutathione-Sepharose beads (GE Bioscience) and BIT1 was released from GST by thrombin cleavage. After purification, BIT1 in PBS (1 mg/ml) was mixed (v:v) with TiterMax-®Gold adjuvant (CytRX Corporation) and 200 µl of the emulsion was injected intramuscularly in brown leghorn hens. Immunization was boosted 3 weeks after the first injection and eggs were collected the following weeks. Egg yolks were stored diluted tenfold in PBS, 0.2% Tween20, 0.05% NaN_3 until used. Scrambled and *BIT1* siRNA were designed, as previously reported (Jan et al., 2004).

Tissue fractionation analyses

Dog pancreatic microsomes were isolated as previously described (Chevet et al., 1999). Dog pancreatic microsomes were solubilized using Tween 20, a high hydrophilic-lipophilic balance (HLB=16.7) (Roper et al., 2000) detergent to generate DRMs. The purification of dog pancreatic ER DRMs was adapted from the method previously described for yeast microsome DRMs (Bagnat et al., 2000; Roper et al., 2000). Briefly, microsomes (500 µg proteins) were solubilized in 50 mM Tris-HCl, pH 7.4, 150 mM NaCl, 5 mM EDTA with a protease inhibitor mixture (1 mM PMSF, 2.5 µg/ml chymostatin, leupeptin, and pepstatin) containing 0.75% Tween-20, on ice for 30 minutes. Sucrose concentration was increased to 40% in the lysate then the resulting mix was overlaid with 500 µl of the same buffer containing 30% sucrose, and 200 µl of the same solution containing 2.5% sucrose. After centrifugation at 50,000 r.p.m. for 140 min in a TL50 rotor, the top fraction was reprocessed the same way. After the second spin, the upper fraction was precipitated with TCA, the 15,000 ***g*** pellet was then washed and resuspended in Laemmli sample buffer (Fig. 1A). Subcellular fractionation studies from rat liver were carried out, as previously described (Bell et al., 2001).

Data analysis

Data were analyzed for homologies using BLAST at the NCBI (http://www.ncbi.nlm.nih.gov). Potential transmembrane domains (TMD) were identified using http://www.cbs.dtu.dk/services/TMHMM-2.0 and Pi and molecular masses computed at http://ca.expasy.org/tools/pi_tool.html. BIT1 homolog sequences were retrieved from Homologene database (NCBI, HomoloGene entry no. 5330). Seventeen protein sequences from various species were aligned using the multiple sequence alignment tool Multalin (version 5.4.1) (Corpet, 1988) and the alignment result was presented as a phylogenetic tree using the phylogeny reconstruction algorithm BIONJ (Gascuel, 1997). The protein sequences from six (representative) species were aligned using CLUSTALW (Thompson et al., 1994) and visualized using the program ESPript (Gouet et al., 2003). Functional network analysis was carried out using the STRING suite program (Snel et al., 2000; von Mering et al., 2003).

Morphological analysis or ER microsomes and quantification

The quality of the ER microsomes was assessed by electron microscopy, as previously described (Lavoie et al., 2000). Microsomes were quantified in 20 different images (1430 microsomes counted) with rough vesicles counted as ER vesicles, and smooth vesicles (devoid of ribosomes) counted as mitochondrial by default.

Cell culture and transfection

Cells were grown in DMEM with 10% FBS (Hyclone). Plasmids pcDNA3.Myc (empty vector), pcDNA3.BIT1, pcDNA3.TrapLT and pcDNA3.Trap.BIT1 were used to transfect FR3T3 cells using Lipofectamine (Invitrogen). Stable transfectants were selected with G418 (400 µg/ml) over a period of 2-3 weeks. Two individual clones from each construct were kept for further studies. Transfection of HuH7 cells was carried out using PromoFectin reagent (PromoKine) following the manufacturer's recommendations.

Proliferation assay

Cells were seeded in triplicate at 20,000 cells/well in 24-well plates and cultured in DMEM containing 10% FBS. Cells were counted after 4 days in culture using a Neubaer hemocytometer.

Immunoprecipitation

Cells were lysed in 20 mM Tris-HCl, pH 8.0, 150 mM NaCl, 1% Triton X-100 (TX), 1 mM NaF, 1 mM Na_3VO_4, 1 mM phenylmethylsulfonyl fluoride (PMSF), and 10 µg/ml leupeptin and aprotinin. Precleared lysates were incubated with anti-MYC antibodies (Upstate) for 16 hours at 4°C followed by incubation with protein G-Sepharose beads (Amersham) for 1 hour at room temperature. Beads were washed three times with PBS, mixed with Laemmli sample buffer, boiled for 3 minutes and spun briefly. Protein complexes present in the resulting supernatant were resolved by SDS-PAGE and analyzed by immunoblot using anti-BIT1 antibodies.

Immunofluorescence analyses

Cells grown in 24-well plates (20,000 cells/coverslip) were fixed with 3.7% formaldehyde for 10 minutes, permeabilized with 0.1% Triton-X 100 for 5 minutes, incubated with anti-Myc or anti-calnexin antibodies for 1 hour at room temperature followed by incubation with anti-rabbit or anti-mouse FITC-conjugated antibodies. Protein immunolocalization was carried out using epifluorescence microscopy with a Zeiss ×63 1.4 NA oil-immersion objective, recorded with a digital camera (DVC) and analyzed with Northern Eclipse software (Emprix imaging), or confocal microscopy with a LEICA SP5 confocal microscope. Determination of the size of the Golgi complex was carried out following staining using anti-giantin antibodies and the 'analyze particles' function was used after thresholding to yield the sum of each Golgi perimeter on a per-cell basis. Three independent experiments were performed.

Subcellular fractionation

Cells (5×10^6 cells/plate) were washed twice with cold PBS, homogenized in 150 mM KCl, 10 mM Tris-HCl, pH 7.5, 2.5 mM magnesium acetate, 0.25 M sucrose, 4 mM imidazole, pH 7.4, 1 mM PMSF, 5 mM NaF, 1 mM Na_3VO_4, complete protease inhibitors cocktail (Roche), homogenized (30 strokes with a Teflon potter) and centrifuged at 1000 ***g*** for 20 minutes at 4°C. The resulting post-nuclear supernatants were fractionated into P10 by centrifugation at 10,000 ***g*** for 30 minutes at 4°C, then into P100 by centrifugation of the resulting supernatant at 100,000 ***g*** for 30 minutes at 4°C in a Beckman TLA-100.2 rotor. Each pellet was resuspended in Laemmli

Journal of Cell Science

sample buffer. Proteins were detected by immunoblotting with anti-BIT1, anti-CNX, anti-Trapα, anti-Tom20 or anti-ERK-1 antibodies.

Soft agar assay

Soft agar assay was done in duplicate using six-well plates. Each well contained 2.5 ml of bottom layer (0.5% agarose in DMEM 10% FBS) and 1.5 ml of top layer (0.2% agarose in DMEM 10% FBS) containing 5000 cells. Cells were fed twice a week by adding 1 ml of top layer without cells. Colonies from ten different fields were counted after two and three weeks in culture by two independent investigators.

Anoikis assay

500,000 cells were cultured in suspension on a 1% agarose bottom layer in DMEM 10% FBS. After 24, 48 or 96 hours, cells were collected and centrifuged at 3000 r.p.m. for 5 minutes. Cells were resuspended in methanol and spread out on a slide. Apoptotic Tunel assay was performed using the in situ cell death detection kit (Roche) according to the manufacturer's instructions. Nuclei were stained with DAPI. More than 500 nuclei from each cell clone were counted and the percentage of apoptotic nuclei calculated.

Semi quantitative RT-PCR

The expression of Bcl2, CHOP and S16 was assessed by semiquantitative RT-PCR as described previously (Nguyen et al., 2004). The following oligonucleotides were used: 5′-TGCACCTGACGCCCTTCAC-3′ and 5′-ACACAGCCAGGAGAAATC-AAACAG-3′ for Bcl2; 5′-GGCAGCTGAGTCTCT-3′ and 5′-GGTGCAGACTG-ACCA-3′ for CHOP; 5′-TGCTGGTGTGGATATTCGGG-3′ and 5′-CCTTGAGA-TGGGCTTATCGG-3′ for S16.

Kinase phosphorylation

Cells were lysed in 20 mM Tris-HCl, pH 8.0, 150 mM NaCl, 1% TX, 1 mM NaF, 1 mM Na_3VO_4, 1 mM PMSF, and 10 μg/ml leupeptin and aprotinin. Lysates were resolved by SDS-PAGE and analyzed by immunoblot using anti-MEK1/2, anti-ERK1/2, anti-PAK1, anti-RAF1 (all from Santa-Cruz Biotechnologies), anti-MEKK-7 and anti-phospho-MEKK-7 (kind gifts from Philip A. Barker, McGill University, Montreal, Canada), anti-phospho-MEK-1/2, anti-phospho-ERK-1/2, anti-phospho-RAF1, anti-phospho-AKT, anti-AKT, anti-phospho-Smad2 (all from Cell Signaling), or anti-Smad2 antibodies (Santa-Cruz).

Sample preparation and mass spectrometry analysis

After resolution of the DRM-associated proteins by SDS-PAGE, and Coomassie R-250 staining, each individual band was cut out and the corresponding slices were dehydrated in acetonitrile and washed by two cycles of 10 minutes in 100 mM $(NH_4)_2CO_3$ before the addition of an equal volume of acetonitrile. The completely destained gel slices were then treated for 30 minutes with 10 mM dithiothreitol to reduce cystinyl residues and for 20 minutes with 55 mM iodoacetamide to effect alkylation. After an additional round of $(NH_4)_2CO_3$ and acetonitrile washes, the slices were extracted with acetonitrile at 37°C. They were then incubated with trypsin (6 ng/μl in 50 mM $[NH_4]_2CO_3$) for 5 hours at 37°C and the peptides were first extracted in 1% formic acid, 2% acetonitrile followed by two further extractions with additions of acetonitrile. All treatments were performed robotically using a MassPrep Workstation (MicroMass). Extracted peptides were applied to a reverse-phase guard column and then eluted in-line to a 10 cm by 75 μm PicoFrit column filled with BioBasic C18. The column was eluted at 200 nl/minute with a linear gradient of 5-70% acetonitrile, 0.1% formic acid. For all peptides, a 30 minute gradient was used. A 2000 V charge was applied to the PicoFrit column such that the eluted peptides are electrosprayed into a Cap liquid chromatography quadrapole time-of-flight MS (MicroMass). When doubly or triply charged ions were detected, the quadrapole was used to select the precursor ion, which was passed into a collision cell where fragmentation was induced by collision with argon gas. The collision energies are determined automatically by the instrument based on the m/z values and charge states of each peptide. Fragmentation data were collected in 1 second scans for up to 5 seconds. The MS/MS data was peaklisted (MassLynx; MicroMass) and submitted to Mascot (MatrixScience) software for database search analysis against the NCBI non-redundant database.

Plasmid construction

A human liver cDNA library was used as a template to PCR amplify either full-length or subfragments of BIT1 and Trap: BIT1 full-length (BIT1, aa 1-179): 5′-GGG GAC AAG TTT GTA CAA AAA AGC AGG CTT GAT GCC CTC CAA ATC CTT GGT TAT G-3′ and 5′-GGG GAC CAC TTT GTA CAA GAA AGC TGG GTT GTA AAG TTT TAG GTG ACC AGT GAC TTT GT-3′. Trapα luminal and transmembrane (TrapLT): 5′-GGG GAC AAG TTT GTA CAA AAA AGC AGG CTT GAT GAG ACT CCT CCC CCG CTT-3′ and 5′-GGG GAC CAC TTT GTA CAA GAA AGC TGG GCA TCA TTC TGA CTT GAT GTA CCC ATT TCT A-3′ for amplification of the predicted luminal and transmembrane domains of Trapα (aa 1-250). Trap.BIT1: 5′-GGG GAC AAG TTT GTA CAA AAA AGC AGG CTT GAT GAG ACT CCT CCC CCG CTT-3′ and 5′-GGC GCC GGC ATC ATT CTG ACT TGA TGT ACC CAT TTC TAC-3′ for amplification of the predicted luminal and transmembrane domains of Trapα followed by an AGA linker sequence (Trapα, aa 1-250; TrapLT-AGA); 5′-GCC GGC GCC CCC AAA AGC AAG ACG AGC AAG-3′ and 5′-GGG GAC CAC TTT GTA CAA GAA AGC TGG GTT GTA AAG TTT TAG GTG ACC AGT GAC TTT GTC A-3′ for amplification of the predicted BIT1 cytosolic domain (aa 41-179) downstream of an AGA linker sequence (AGA-BIT1cyto). TrapLT-AGA and AGA-BIT1cyto (aa 41-179) fragments were gel-purified, mixed and subjected to a second round of PCR amplification with 5′-GGG GAC AAG TTT GTA CAA AAA AGC AGG CTT GAT GAG ACT CCT CCC CCG CTT-3′ (Trapα Fwd Gateway compatible) and 5′-GGG GAC CAC TTT GTA CAA GAA AGC TGG GTT GTA AAG TTT TAG GTG ACC AGT GAC TTT GTC A-3′ (BIT1 Rev Gateway compatible) to generate a DNA fragment encoding a Trap.BIT1 fusion protein with a Ala-Gly-Ala linker sequence. All PCR products were amplified using HiFi polymerase (Invitrogen) and then inserted into the pDONR201 vector by recombinational cloning (GATEWAY, Invitrogen). The resulting plasmids were then recombined into pCDNA3-Myc His (Cterm) that had been previously made GATEWAY compatible (Invitrogen) to generate C-terminally tagged full-length BIT1, TrapLT and Trap.BIT1.

We thank the Chevet lab for discussions and critical advice. We are grateful to Philip A. Barker (McGill University, Montreal, Canada) for the anti-phospho-MKK7 and anti-MKK7 antibodies. This work was supported by grants from INSERM (AVENIR), Institut National du Cancer, la Fondation pour la Recherche Médicale and the European Community (Marie Curie International reintegration grant) to E.C. and by a Génome Québec/Génome Canada Grant to the Cell Map Project. P.Y. was supported by a 'poste vert' from INSERM.

Supplementary material available online at
http://jcs.biologists.org/cgi/content/full/123/7/1060/DC1

References

Bagnat, M., Keranen, S., Shevchenko, A. and Simons, K. (2000). Lipid rafts function in biosynthetic delivery of proteins to the cell surface in yeast. *Proc. Natl. Acad. Sci. USA* **97**, 3254-3259.

Bell, A. W., Ward, M. A., Blackstock, W. P., Freeman, H. N., Choudhary, J. S., Lewis, A. P., Chotai, D., Fazel, A., Gushue, J. N., Paiement, J. et al. (2001). Proteomics characterization of abundant Golgi membrane proteins. *J. Biol. Chem.* **276**, 5152-5165.

Berridge, M. J. (2002). The endoplasmic reticulum: a multifunctional signaling organelle. *Cell Calcium* **32**, 235-249.

Bickel, P. E. (2002). Lipid rafts and insulin signaling. *Am. J. Physiol. Endocrinol. Metab.* **282**, E1-E10.

Biliran, H., Jan, Y., Chen, R., Pasquale, E. B. and Ruoslahti, E. (2008). Protein kinase D is a positive regulator of Bit1 apoptotic function. *J. Biol. Chem.* **283**, 28029-28037.

Brandlin, I., Hubner, S., Eiseler, T., Martinez-Moya, M., Horschinek, A., Hausser, A., Link, G., Rupp, S., Storz, P., Pfizenmaier, K. et al. (2002). Protein kinase C (PKC)eta-mediated PKC mu activation modulates ERK and JNK signal pathways. *J. Biol. Chem.* **277**, 6490-6496.

Brown, D. A. and London, E. (1998). Functions of lipid rafts in biological membranes. *Annu. Rev. Cell Dev. Biol.* **14**, 111-136.

Chevet, E., Wong, H. N., Gerber, D., Cochet, C., Fazel, A., Cameron, P. H., Gushue, J. N., Thomas, D. Y. and Bergeron, J. J. (1999). Phosphorylation by CK2 and MAPK enhances calnexin association with ribosomes. *EMBO. J.* **18**, 3655-3666.

Corpet, F. (1988). Multiple sequence alignment with hierarchical clustering. *Nucleic Acids Res.* **16**, 10881-10890.

Doan, J. E., Windmiller, D. A. and Riches, D. W. (2004). Differential regulation of TNF-R1 signaling: lipid raft dependency of p42mapk/erk2 activation, but not NF-kappaB activation. *J. Immunol.* **172**, 7654-7660.

Fan, T., Jiang, G., Suo, Z., Liu, H., Xu, P., Ji, Z., Zhang, L. and Yang, G. (2009). Down-regulation of the apoptosis-inducing factor or Bcl-2 inhibitor of transcription by RNA interference can alleviate TAp63gamma-induced apoptosis in esophageal squamous carcinoma EC9706 cells. *Int. J. Oncol.* **35**, 359-367.

Foyouzi-Youssefi, R., Arnaudeau, S., Borner, C., Kelley, W. L., Tschopp, J., Lew, D. P., Demaurex, N. and Krause, K. H. (2000). Bcl-2 decreases the free Ca^{2+} concentration within the endoplasmic reticulum. *Proc. Natl. Acad. Sci. USA* **97**, 5723-5728.

Gascuel, O. (1997). BIONJ: an improved version of the NJ algorithm based on a simple model of sequence data. *Mol. Biol. Evol.* **14**, 685-695.

Germain, M. and Shore, G. C. (2003). Cellular distribution of Bcl-2 family proteins. *Sci STKE* **2003**, 10.

Ghanekar, Y. and Lowe, M. (2005). Protein kinase D: activation for Golgi carrier formation. *Trends. Cell Biol.* **15**, 511-514.

Gilchrist, A., Au, C. E., Hiding, J., Bell, A. W., Fernandez-Rodriguez, J., Lesimple, S., Nagaya, H., Roy, L., Gosline, S. J., Hallett, M. et al. (2006). Quantitative proteomics analysis of the secretory pathway. *Cell* **127**, 1265-1281.

Gouet, P., Robert, X. and Courcelle, E. (2003). ESPript/ENDscript: Extracting and rendering sequence and 3D information from atomic structures of proteins. *Nucleic Acids Res.* **31**, 3320-3323.

Gu, F., Nguyen, D. T., Stuible, M., Dube, N., Tremblay, M. L. and Chevet, E. (2004). Protein-tyrosine phosphatase 1B potentiates IRE1 signaling during endoplasmic reticulum stress. *J. Biol. Chem.* **279**, 49689-49693.

Harder, T. (2004). Lipid raft domains and protein networks in T-cell receptor signal transduction. *Curr. Opin. Immunol.* **16**, 353-359.

Hausser, A., Storz, P., Martens, S., Link, G., Toker, A. and Pfizenmaier, K. (2005). Protein kinase D regulates vesicular transport by phosphorylating and activating phosphatidylinositol-4 kinase IIIbeta at the Golgi complex. *Nat. Cell. Biol.* **7**, 880-886.

Ikonen, E. and Simons, K. (1998). Protein and lipid sorting from the trans-Golgi network to the plasma membrane in polarized cells. *Semin. Cell Dev. Biol.* **9**, 503-509.

Inder, K., Harding, A., Plowman, S. J., Philips, M. R., Parton, R. G. and Hancock, J. F. (2008). Activation of the MAPK module from different spatial locations generates distinct system outputs. *Mol. Biol. Cell* **19**, 4776-4784.

Jan, Y., Matter, M., Pai, J. T., Chen, Y. L., Pilch, J., Komatsu, M., Ong, E., Fukuda, M. and Ruoslahti, E. (2004). A mitochondrial protein, Bit1, mediates apoptosis regulated by integrins and Groucho/TLE corepressors. *Cell* **116**, 751-762.

Kairouz-Wahbe, R., Biliran, H., Luo, X., Khor, I., Wankell, M., Besch-Williford, C., Pascual, J., Oshima, R. and Ruoslahti, E. (2008). Anoikis effector Bit1 negatively regulates Erk activity. *Proc. Natl. Acad. Sci. USA* **105**, 1528-1532.

Kubler, E., Dohlman, H. G. and Lisanti, M. P. (1996). Identification of Triton X-100 insoluble membrane domains in the yeast Saccharomyces cerevisiae. Lipid requirements for targeting of heterotrimeric G-protein subunits. *J. Biol. Chem.* **271**, 32975-32980.

Lavoie, C., Chevet, E., Roy, L., Tonks, N. K., Fazel, A., Posner, B. I., Paiement, J. and Bergeron, J. J. (2000). Tyrosine phosphorylation of p97 regulates transitional endoplasmic reticulum assembly in vitro. *Proc. Natl. Acad. Sci. USA* **97**, 13637-13642.

Legler, D. F., Micheau, O., Doucey, M. A., Tschopp, J. and Bron, C. (2003). Recruitment of TNF receptor 1 to lipid rafts is essential for TNFalpha-mediated NF-kappaB activation. *Immunity* **18**, 655-664.

Lunin, V. V., Munger, C., Wagner, J., Ye, Z., Cygler, M. and Sacher, M. (2004). The structure of the MAPK scaffold, MP1, bound to its partner, p14. A complex with a critical role in endosomal map kinase signaling. *J. Biol. Chem.* **279**, 23422-23430.

Miljan, E. A. and Bremer, E. G. (2002). Regulation of growth factor receptors by gangliosides. *Sci STKE* **2002**, RE15.

Mor, A. and Philips, M. R. (2006). Compartmentalized Ras/MAPK signaling. *Annu. Rev. Immunol.* **24**, 771-800.

Morgado-Diaz, J. A., Montesano, G., De Souza Fernandes, S., Redondo, P. A., Fernandes de Souza, W., Albuquerque-Xavier, A. C., Leve, F., Tanaka, M. N., Martins de Araujo, W., Oliveira, S. S. et al. (2007). Golgi complex disassembly caused by light-activated calphostin C involves MAPK and PKA. *Tissue Cell* **39**, 161-169.

Nguyen, D. T., Kebache, S., Fazel, A., Wong, H. N., Jenna, S., Emadali, A., Lee, E. H., Bergeron, J. J., Kaufman, R. J., Larose, L. et al. (2004). Nck-dependent activation of extracellular signal-regulated kinase-1 and regulation of cell survival during endoplasmic reticulum stress. *Mol. Biol. Cell* **15**, 4248-4260.

Philips, M. R. (2004). Sef: a MEK/ERK catcher on the Golgi. *Mol. Cell* **15**, 168-169.

Roper, K., Corbeil, D. and Huttner, W. B. (2000). Retention of prominin in microvilli reveals distinct cholesterol-based lipid micro-domains in the apical plasma membrane. *Nat. Cell Biol.* **2**, 582-592.

Rudner, J., Jendrossek, V. and Belka, C. (2002). New insights in the role of Bcl-2 Bcl-2 and the endoplasmic reticulum. *Apoptosis* **7**, 441-447.

Sanchez-Ruiloba, L., Cabrera-Poch, N., Rodriguez-Martinez, M., Lopez-Menendez, C., Jean-Mairet, R. M., Higuero, A. M. and Iglesias, T. (2006). Protein kinase D intracellular localization and activity control kinase D-interacting substrate of 220-kDa traffic through a postsynaptic density-95/discs large/zonula occludens-1-binding motif. *J. Biol. Chem.* **281**, 18888-18900.

Schneider-Brachert, W., Tchikov, V., Neumeyer, J., Jakob, M., Winoto-Morbach, S., Held-Feindt, J., Heinrich, M., Merkel, O., Ehrenschwender, M., Adam, D. et al. (2004). Compartmentalization of TNF receptor 1 signaling: internalized TNF receptosomes as death signaling vesicles. *Immunity* **21**, 415-428.

Schroder, M. and Kaufman, R. J. (2005). The mammalian unfolded protein response. *Annu. Rev. Biochem.* **74**, 739-789.

Smith, D. C., Sillence, D. J., Falguieres, T., Jarvis, R. M., Johannes, L., Lord, J. M., Platt, F. M. and Roberts, L. M. (2006). The association of Shiga-like toxin with detergent-resistant membranes is modulated by glucosylceramide and is an essential requirement in the endoplasmic reticulum for a cytotoxic effect. *Mol. Biol. Cell* **17**, 1375-1387.

Snel, B., Lehmann, G., Bork, P. and Huynen, M. A. (2000). STRING: a web-server to retrieve and display the repeatedly occurring neighbourhood of a gene. *Nucleic Acids Res.* **28**, 3442-3444.

Stitziel, N. O., Mar, B. G., Liang, J. and Westbrook, C. A. (2004). Membrane-associated and secreted genes in breast cancer. *Cancer Res.* **64**, 8682-8687.

Thompson, J. D., Higgins, D. G. and Gibson, T. J. (1994). CLUSTAL W: improving the sensitivity of progressive multiple sequence alignment through sequence weighting, position-specific gap penalties and weight matrix choice. *Nucleic Acids Res.* **22**, 4673-4680.

von Mering, C., Huynen, M., Jaeggi, D., Schmidt, S., Bork, P. and Snel, B. (2003). STRING: a database of predicted functional associations between proteins. *Nucleic Acids Res.* **31**, 258-261.

Wong, C. and Jin, Z. G. (2005). Protein kinase C-dependent protein kinase D activation modulates ERK signal pathway and endothelial cell proliferation by vascular endothelial growth factor. *J. Biol. Chem.* **280**, 33262-33269.

Zhang, X. and Thompson, G. A., Jr (1997). An apparent association between glycosylphosphatidylinositol-anchored proteins and a sphingolipid in Tetrahymena mimbres. *Biochem. J.* **323**, 197-206.

Journal of Cell Science